High-energy radiation monitoring based on radio-fluorogenic co-polymerization. I: small volume *in situ* probe

2009 Phys. Med. Biol. 54 3185

(http://iopscience.iop.org/0031-9155/54/10/015)

IOP PUBLISHING PHYSICS IN MEDICINE AND BIOLOGY

Phys. Med. Biol. **54** (2009) 3185–3200 doi:10.1088/0031-9155/54/10/015

High-energy radiation monitoring based on radio-fluorogenic co-polymerization. I: small volume *in situ* probe

J M Warman, M P de Haas and L H Luthjens

Reactor Institute R3/RIH, Technical University of Delft, Mekelweg 15, 2629 JB Delft, The Netherlands

E-mail: J.M.Warman@TUDelft.NL

Received 10 February 2009, in final form 29 March 2009
Published 6 May 2009
Online at stacks.iop.org/PMB/54/3185

Abstract

A method of radiation dosimetry is described which is based on the radiation-induced initiation of polymerization of a bulk monomer (e.g. methyl methacrylate) containing a small concentration (about 100 ppm) of a compound which is non-fluorescent but which becomes highly fluorescent when it is incorporated into a growing polymer chain of the bulk monomer. We call the overall process 'radio-fluorogenic co-polymerization' or RFCP for short. The method is illustrated by results on the *in situ* monitoring of the accumulated dose within the irradiation chamber of a cobalt-60 gamma-ray source using a small plastic capsule containing about 0.2 ml of an RFCP solution. Remote monitoring of the fluorescence is carried out on a timescale of seconds using optical fibres connecting the probe to a 360 nm LED excitation source and a miniature spectrophotometer. The fluorescence is permanent and the intensity is linearly proportional to the accumulated dose from a few tenths of a gray up to hundreds of gray. The sensitivity to dose depends on the polymerizable monomer used and obeys a square root dependence on dose rate over the range studied, 0.27–3.76 Gy min^{-1}. The polymeric nature of the fluorescent product suggests that the RFCP effect could be used to provide fixed two- or three-dimensional fluorescent images of dose deposition in gel films or phantoms.

1. Introduction

The ability to measure accurately the dose delivered to a material by high energy 'ionizing' radiation is essential in areas such as radiotherapy, radiation processing, radiation sterilization and radiation protection. The dosimetric methods most commonly used are based on gaseous ionization chambers, solid-state diodes, thermally or optically stimulated luminescent solids or radiochromic films. The pros and cons of the different dosimetric methods applied in

the area of radiotherapy have been reviewed recently by d'Errico (2006), Jordan (2006) and Schreiner (2006). In the context of the present optical method of measurement, specific reviews of devices based on radio-luminescence (Beddar 2007), optically stimulated luminescence (Yukihara and McKeever 2008) and radiochromicity (Niroomand-Rad *et al* 1998) are relevant. Of particular importance are the advances that have been made in increasing the sensitivity of radiochromic thin films which are now capable of dose monitoring within the range relevant to radiotherapeutic treament procedures (Soares 2006).

In this paper, we present results on a novel type of dosimetric medium based on 'radio-fluorogenic co-polymerization' or RFCP. In this method, the active medium consists of a liquid monomer that polymerizes on exposure to high-energy radiation. Dissolved in the bulk monomer is a small concentration of a compound that is normally non-fluorescent but becomes fluorescent when incorporated into a growing polymer chain of the monomer. The intensity of the fluorescence of the medium after irradiation is proportional to the total yield of initiating free radicals formed and hence to the accumulated radiation dose.

A radio-fluorogenic medium based on an aqueous solution of coumarin-3-carboxylic acid has previously been demonstrated (Collins *et al* 1994, Park *et al* 2006). This also results in the formation of a permanent fluorescent product proportional to the accumulated radiation dose. The method presented here has two distinct advantages over the coumarin-based method, both of which are due to the polymerization process underlying RFCP. Firstly, for every reactive free radical formed by irradiation, thousands to hundreds of thousands of monomeric molecules are incorporated into the resulting polymer chains. This results in an amplification factor that increases the effective yield of the fluorescescent product. Secondly, the fluorescent product is a high molecular weight polymer with a very much smaller diffusion coefficient than the small-molecule product of the coumarin-based dosimeter. This opens up the possibility of applying the RFCP effect within a semi-rigid gel matrix to provide two- or even three-dimensional fluorescent images of dose distribution. This could add to the armoury of 3D gel-dosimetry methods already in existence (Collomb-Patton *et al* 2009, Ibbott 2006, De Deene 2006, Doran and Krstajic 2006).

The RFCP effect was first demonstrated by one of the present authors (Warman *et al* 1997). It was subsequently applied to the study of radiation-induced polymerization with particular attention to the sudden auto-acceleration of polymerization in methyl methacrylate (Warman *et al* 1999, Frahn *et al* 2001, 2003, 2004). This occurs at relatively high monomer conversions and correspondingly high gamma-ray doses on the order of kilogray. The authors recently decided to investigate whether the RFCP effect could be applied as a dosimetric method in the lower dose linear range of monomer conversion. A short publication of the initial results will appear in the conference proceedings of DOSGEL 2008 (Warman *et al* 2009). In the present paper, we describe in greater detail the experimental apparatus and procedures used. In addition, we demonstrate how the sensitivity of the method can be dramatically influenced by the choice of the bulk monomer used. The results reported here are limited to *in situ* measurements in a cobalt gamma-ray irradiator using a small volume RFCP probe solution. Future papers in this series will be concerned with RFCP gels and results obtained on 2D and 3D fluorescent images of radiation beams.

2. Experimental details

2.1. Materials

The radiation-polymerizable bulk monomers used were methyl methacrylate, MMA (Aldrich 99%), and tertiary-butyl acrylate, tBuA (Scientific Polymer Products or Fluka purum). The

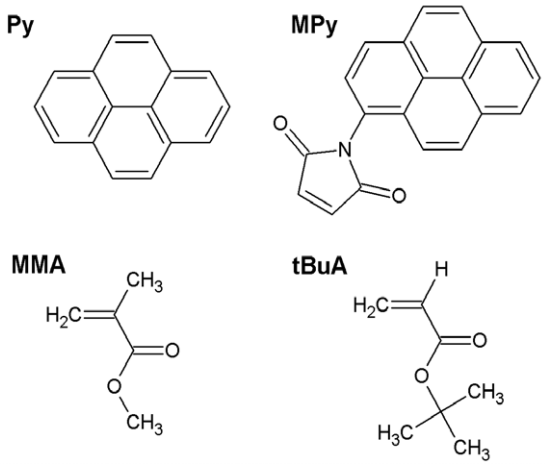

Figure 1. The molecular structures of pyrene (Py) and its fluorogenic derivative *N*-(1-pyrenyl)maleimide (MPy). Also shown are the structures of the radiation-polymerizable monomers methyl methacrylate (MMA) and tertiary-butyl acrylate (tBuA).

molecular structures are shown in figure 1. The hydroquinone stabilizer was removed by passage over the DHR-4 removal columns provided. The purified liquids were stored in the dark at 5 °C. The gravimetric density and the electron density relative to water of the monomer liquids are 0.94 g cm^{-3} and 0.92 for MMA and 0.87 g cm^{-3} and 0.86 for tBuA, respectively. Both liquids are therefore close to soft tissue equivalent with respect to energy deposition by high-energy electron or photon radiation.

The fluorogenic compound used in the present work was *N*-(1-pyrenyl)maleimide, 'MPy' (Invitrogen SKU P-28 or Sigma P7908). The molecular structure of MPy is shown in figure 1 together with unsubstituted pyrene, Py. Solutions of MPy in the above monomers on the order of millimolar concentration (about 100 ppm) were made and the optical densities were measured using a Uvikon 940 spectrophotometer (Kontron Instruments). In the measurements reported here the optical densities of the solutions at the excitation wavelength of 360 nm were approximately 2 cm^{-1}. The extinction coefficient of MPy at 360 nm is 930 M^{-1} cm^{-1} in MMA.

The fluorogenic solution was contained in a hollow 25 mm long, 8.5 mm outer diameter cylinder of either poly-tetrafluoroethylene, 'PTFE', or polyethylene, 'PE'. The gravimetric density and electron density relative to water of these materials are 2.2 g cm^{-3} and 1.89 for PTFE, and 0.96 g cm^{-3} and 0.94 for PE, respectively. The cavity containing the solution within the cylinder was 10 mm long and 4.5 mm in diameter, corresponding to a volume of 0.16 ml. In what follows the plastic cylinder filled with the fluorogenic solution is referred to as the 'probe'.

2.2. Oxygen removal

Of extreme importance for obtaining reproducible results with no initial inhibition period is the complete removal of oxygen from the solution. This was achieved using a glove box (PlasLabs 818GB) that was continuously flushed with pure, dry nitrogen from the institute's continuous, on-tap supply. The fluorogenic solution was purged for 30 min with nitrogen in the glove box prior to pipetting it into the PTFE or PE container. The optical fibre cable,

which was also present within the glove box, was inserted into the cylinder containing the solution with excess solution being exuded via a small (0.4 mm diameter) overflow hole which was automatically shut off when insertion was complete. After removal from the glove box, the probe and cable attachment were wrapped in parafilm as an additional precaution against diffusion of air into the active probe volume. All irradiation measurement procedures were completed within 6 h of removing the probe from the glove box.

2.3. Optical equipment

The optical cable connected to the probe (Avantes, 'FCR-7UV200-2-ME') consisted of a central 200 μm uvasil fibre surrounded by six 200 μm fibres. One metre from the probe, the cable was split into two separate 1 m long cables. One, containing the six outer fibres, was attached to the excitation light source. The other, containing the central fibre, was attached to the input of the spectrophotometer. A schematic diagram of the apparatus is found in Warman *et al* (2009).

The excitation light source was a light-emitting diode (LED, Avantes 'AvaLight-LED-360') with a maximum output in the near UV at 360 nm. The low-level visible tail of the LED emission was cut off above 400 nm using an in-line filter holder (Avantes, 'FH-Inline-UV/Vis-VAR') containing a 3 mm thick UG11 filter.

Light emitted from within the probe was detected using a miniature spectrophotometer (Ocean Optics, 'SD2000'). The output of the spectrophotometer in counts, C, at a given pixel in the detector array, corresponding to a wavelength, λ, was fed to a personal computer (Apple 'MacBook'). One count corresponded to approximately 100 photons absorbed by a pixel, each of which was individually calibrated. Using the accompanying software (Ocean Optics, 'SpectraSuite'), the output could be integrated over a user definable period Δt and spectra of the intensity of the emission, defined as $I(\lambda) = C(\lambda)/\Delta t$, over the wavelength range from 200 to 800 nm could be taken and stored at given times. In addition, the average intensity between user-defined wavelength limits, $\langle I\rangle(\lambda_1 - \lambda_2)$, could be automatically determined as a function of elapsed time providing a 'history' of the emission intensity, $\langle I\rangle(t)$. The data could be displayed and stored after every integration period, Δt, or multiples of it. The values of Δt used in the present work were between 2 and 20 s.

2.4. Radiation source

Irradiations were carried out using a cobalt-60 gamma ray source (Atomic Energy of Canada, 'Gammacell 200'). The source and optical cable transport lock are illustrated in figure 2 of Warman *et al* (1999). The probe was centrally placed in the sample chamber of the source prior to being mechanically lowered into the irradiation zone of the irradiator, which automatically started the source timer. The unattenuated dose rate in the irradiation zone was accurately known from Fricke dosimetry and was routinely corrected for the 5.272 year half-life of cobalt-60. During the period of the measurements reported here, the dose rate decreased from 3.76 to 3.73 Gy min^{-1}. The dose rate at the centre of the chamber could be reduced by factors of 4.2 and 14 using cylindrical lead attenuators. The dimensions of the attenuators were height 135 mm, outer diameter 85 mm and inner diameters 48 mm and 15 mm, respectively.

3. Results and discussion

In figure 2, the molecular mechanism underlying RFCP is illustrated. The conversion of the carbon–carbon double bond of the maleimido group of MPy into a single carbon–carbon

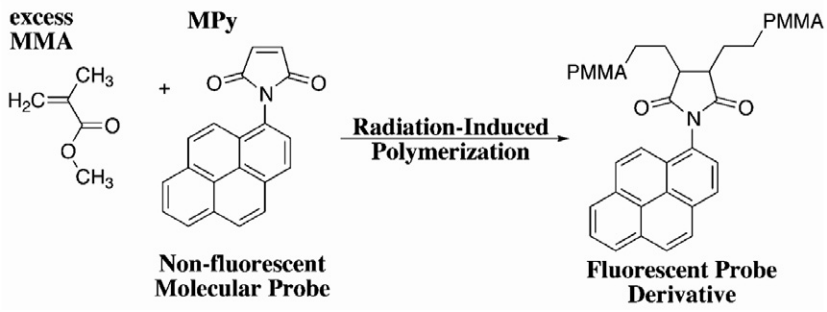

Figure 2. The underlying mechanism of radio-fluorogenic co-polymerization (RFCP) in a dilute solution of MPy in MMA.

bond on incorporation of MPy into a growing chain of the acrylate is the chemical change responsible for the increase in fluorescence of the solution on irradiation. It is important to realize that the fluorescent molecule formed is a high molecular weight polymer into which MPy moieties are incorporated. The average molecular weights of the polymers formed under the present radiation conditions vary from a few hundred kilodalton for MMA up to several megadalton for tBuA, i.e. chains on the order of 100 000 monomer units long. The diffusion coefficient of the fluorescent moiety is therefore considerably reduced compared with that of a freely diffusing MPy molecule. This is particularly important for applications envisaged in which RFCP gels are used for 2D and 3D fluorescent dose imaging.

3.1. Spectrally resolved emission

In the present study, the interest lies in the increase with radiation dose of the intensity of the fluorescence from co-polymerized molecules of the fluorogenic probe molecule MPy. Preliminary, spectrally resolved measurements are required in order to decide over which wavelength region to average the emission data in order to optimize the signal-to-noise ratio.

In figure 3 are shown the emission spectra from a probe containing a fresh solution of MPy in MMA before irradiation, and after a total dose of 600 Gy. Prior to irradiation, a relatively small emission is observed at wavelengths below 400 nm. This can be attributed to a remnant of the excitation light at 360 nm and possibly a spurious amount of unsubstituted pyrene. The much larger structured emission extending into the visible (>400 nm), found after irradiation, is attributed to the fluorescence from the co-polymerized molecules of MPy.

On lowering the probe into the irradiation zone, a prompt additional emission appears as shown in figure 4(A). This reversibly disappears when the probe is raised. The spectrum of this prompt emission, obtained by subtracting the spectrum with the sample chamber raised from that determined immediately on being lowered, is shown in figure 4(B). As can be seen, it is extremely broad with a maximum close to 500 nm. This is attributed to radio-luminescence plus possibly a contribution from Cerenkov radiation from the probe and optical fibres.

On the basis of the spectral information, it was decided to monitor the probe emission by averaging the output of the spectrometer over the wavelength range from 370 nm to 440 nm. This average intensity is denoted by $\langle I \rangle$.

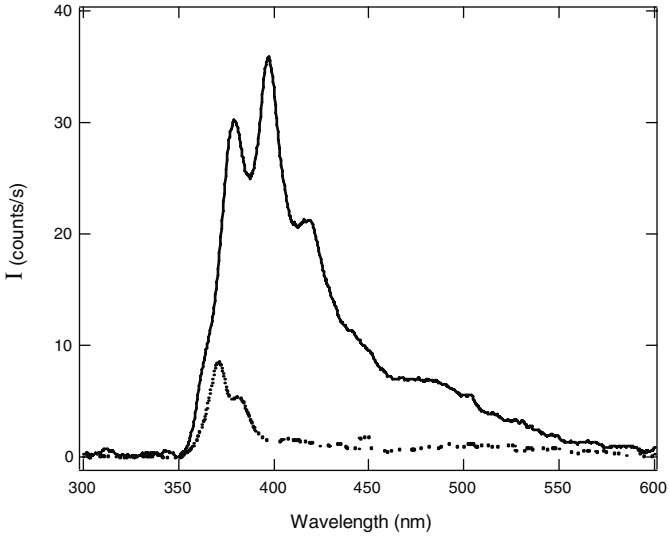

Figure 3. The spectra of the emission from a probe solution of MPy in MMA prior to irradiation, lower spectrum and after a dose of 600 Gy, upper spectrum. The intensity I is the spectrometer output in counts divided by the integration period, Δt, which was 10 s (see section 2.3).

3.2. Emission histories

The history of the average intensity, $\langle I \rangle$, from a freshly prepared solution of MPy in MMA is shown in figure 5. This begins with the sample chamber containing the probe in the raised, i.e. unirradiated, position. At this stage, the chamber contained the 14× lead attenuator (dose rate 0.27 Gy min^{-1}). The initial constant level corresponds to the small background emission of the unirradiated solution in the 370–440 nm region shown in figure 3.

After 10 min, the sample chamber was lowered into the irradiation zone (denoted by 'L' in figure 5). This resulted in a prompt initial increase in emission, mentioned in the previous section, followed by a linear growth with time for the 1 h period when the probe remained in the irradiation zone. On raising the chamber (denoted by 'R' in figure 5), a prompt decrease in emission was found equal in magnitude to the initial prompt increase. The intensity then remained constant during the subsequent period of 10 min when the chamber was raised.

While the chamber was raised, the probe was removed, and the 14× attenuator was exchanged for the 4.2× attenuator (dose rate 0.90 Gy min^{-1}). The probe was then replaced and the chamber was lowered again for a second irradiation period of 1 h. As before, this resulted in a prompt increase in emission followed by a gradual linear growth and a prompt decrease on subsequently raising the probe. During the 10 min period when the chamber was raised, the 4.2× attenuator was removed and the chamber was lowered again with no attenuator present (dose rate 3.76 Gy min^{-1}) for an irradiation time of approximately 4 h, corresponding to an accumulated dose of 1.0 kGy. Only the first 60 min of this period are displayed in figure 5.

As mentioned in the previous section, the prompt increase and decrease in the emission on lowering and raising the probe are attributed to radio-luminescence from the silica optical fibres together with a possible contribution from Cerenkov radiation. The subsequent gradual growth during the 1 h irradiation exposure period is due to the radio-fluorogenic co-polymerization

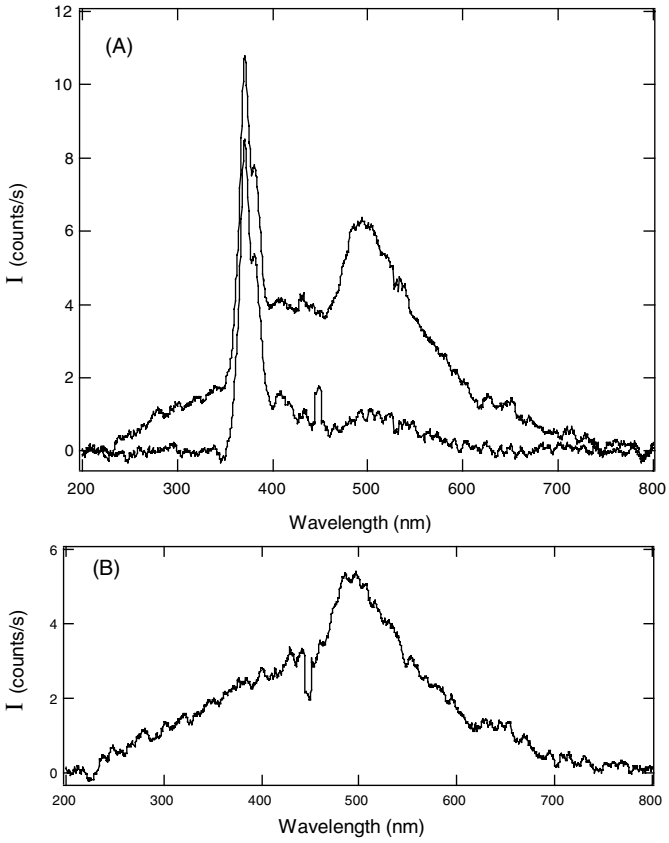

Figure 4. (A) The emission spectra prior to and immediately after (upper spectrum) lowering the probe containing a solution of MPy in MMA into the irradiation zone of the gamma-ray source. (B) The spectrum of the 'prompt' emission obtained by subtraction of the spectra in (A). The intensity I is the spectrometer output in counts divided by the integration period, Δt, which was 10 s (see section 2.3).

effect. When a blank solution containing no MPy was used, only the prompt increase and decrease were found, with a constant level of $\langle I \rangle$ in between.

From the overall history in figure 5, one can clearly see that the slope of the (linear) growth during the hour-long periods of irradiation increases with increasing dose rate, as expected. Furthermore, during the periods when the chamber is raised, the intensity remains close to constant indicating post-irradiation effects to be minimal.

In figure 6(A), a history is shown for a solution of MPy in tBuA carried out in an analogous way to that for MMA in figure 5 and using the same integration time of $\Delta t = 20$ s. As can be seen, the slopes $\mathrm{d}\langle I \rangle / \mathrm{d}t$ for a given dose rate are very much larger for the tBuA solution. Because of this the irradiation exposure times were reduced from the 60 min used for MMA to 10 min for the tBuA solution. The much greater sensitivity of the tBuA solution meant that data with a reasonable signal-to-noise ratio could even be obtained using a considerably reduced integration time. This is shown in figure 6(B), for which Δt was only 2 s. The noise now becomes clearly visible but the slopes can be seen to be close to those in figure 6(A) for

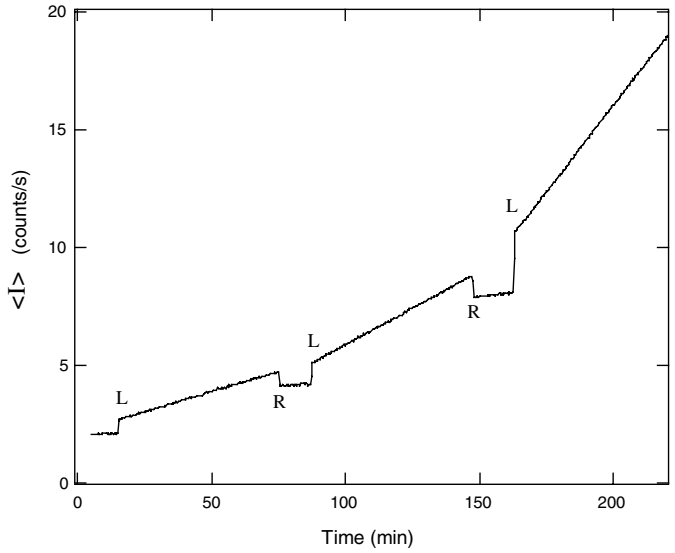

Figure 5. History of the average emission intensity, $\langle I \rangle$ (see section 3.1), for a solution of MPy in MMA beginning in the unirradiated, raised position. The symbols L and R indicate the moments at which the probe was lowered into or raised from the irradiation zone of the source, respectively. The dose rates for the three successive 60 min radiation exposures were 0.27, 0.90 and 3.76 Gy min^{-1}. The integration period, Δt, was 20 s.

which a ten times longer integration time was used. The influence of integration time on the overall accuracy of the measurements will be discussed in the following section.

In order to investigate post-irradiation effects, the probe was allowed to remain in the unirradiated (raised) position for 10 min after a given period of exposure, i.e. after the moment indicated by R in figures 6(A) and (B). As can be seen, after the initial exposure at the lowest dose rate, no significant post-irradiation growth in emission is observed. A slight increase is apparent after exposure at the intermediate dose rate, and after exposure at the highest dose rate, a significant post-irradiation increase of approximately 5% is found. These observations can be explained by a small concentration of free radical species that have not undergone termination during the irradiation period and continue to undergo polymerizaton for some time afterwards. That this effect is largest for the highest dose-rate exposure is to be expected since 14 times more radicals are formed during this irradiation period than that for the lowest dose rate. Clearly this post-irradiation effect will have to be subjected to further investigation, particularly if RFCP probes are to be monitored at a later time after irradiation, i.e. without real-time measurement using optical cables.

3.3. Normalization of histories

In order to obtain information on the fluorogenic effect alone from the elapsed time histories shown in figures 5, 6(A) and (B), we have used the following data handling procedure. For a given irradiation period, time zero is taken as the time of lowering the probe into the irradiation zone, t_L, as defined by the starting of the automatic timer of the source. The irradiation time, t_{rad}, is then given by $t_{\mathrm{rad}} = (t - t_L)$. To derive the value of the intensity due to RFCP fluorescence alone, $\Delta\langle I \rangle$, the measured value, $\langle I \rangle(t)$, must be corrected for the contributions

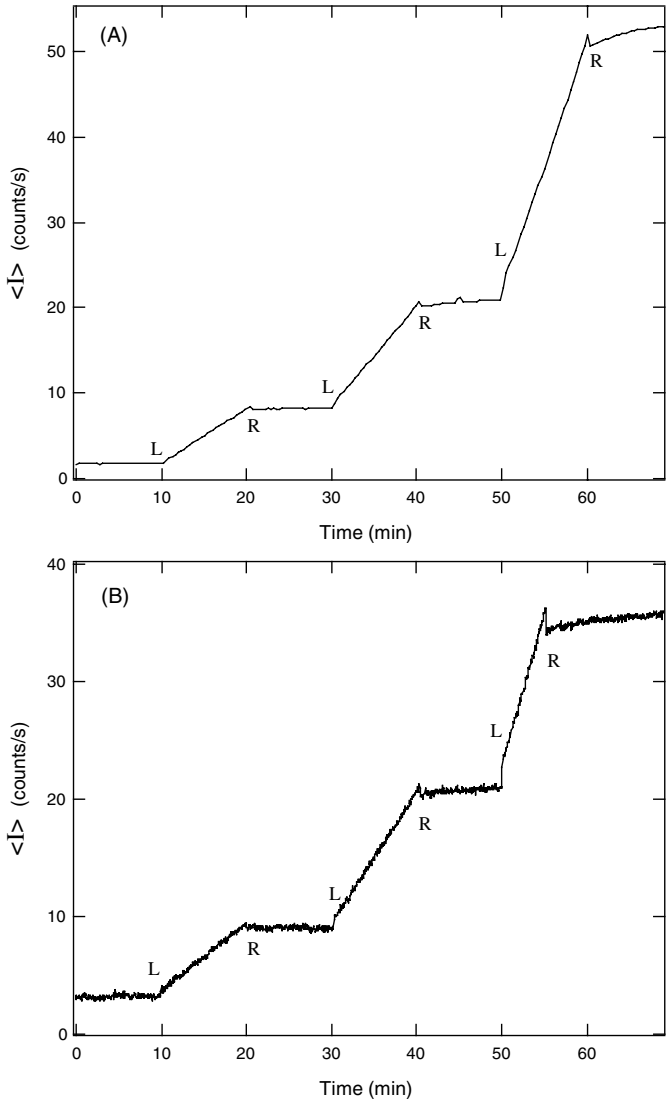

Figure 6. History of the average emission intensity, $\langle I \rangle$ (see section 3.1), for solutions of MPy in tBuA with successive dose rates of 0.27, 0.89 and 3.73 Gy min^{-1}. (A) Three irradiation periods of 10 min; $\Delta t = 20$ s. (B) Irradiation periods of 10, 10 and 5 min; $\Delta t = 2$ s. The symbols L and R indicate the moments at which the probe was lowered into or raised from the irradiation zone of the source.

from the background and prompt emissions. In the present work, this has been done after the fact by extrapolating the value of the linear growth of $\langle I \rangle(t)$ back to $t = t_L$ and subtracting this from the $\langle I \rangle(t)$ values in the database for times longer than t_L. An automated software version of this procedure could be created that would allow continuous, real-time output of $\Delta\langle I \rangle$ versus $(t - t_L)$ after a delay corresponding to a few Δt periods.

The $\Delta\langle I \rangle$ versus irradiation time plots obtained from the histories in figures 5, 6(A) and (B) are shown in figures 7, 8(A) and (B), respectively. In all cases the plots are found to display

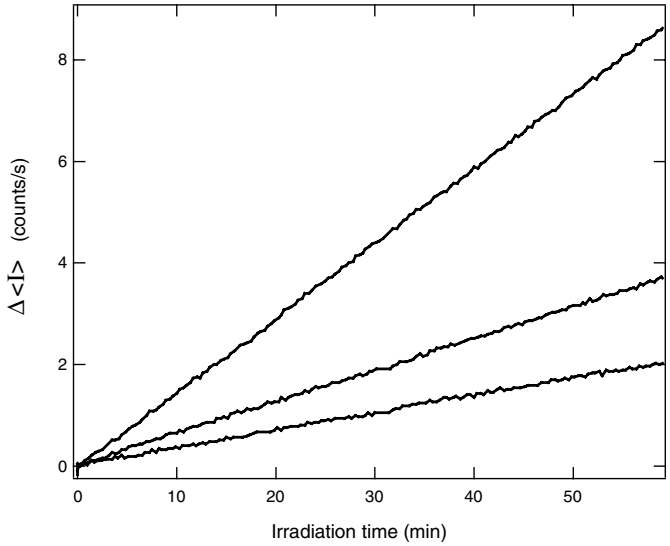

Figure 7. The increase in the fluorescence intensity, $\Delta\langle I\rangle$ (see section 3.3), as a function of time after lowering the probe into the irradiation zone for a solution of MPy in MMA with $\Delta t = 20$ s and dose rates of 3.76, 0.90 and 0.27 Gy min^{-1} (from top to bottom). The total accumulated doses were 226, 54 and 16 Gy, respectively.

a good linear behaviour over the time period measured: 60 min for figure 7 and 5 min for figures 8(A) and (B). In addition, all plots, including the initial lowest dose rate dependences, pass through zero at zero time. This lack of an inhibition period supports the efficacy of the deaeration procedure used. The maximum monomer conversions corresponding to the largest dose rates in figures 7 and 8 were 5% and 8%, respectively. The dependence of the slopes of the plots on dose rate is discussed in section 3.5.

As is apparent from the data in figures 8(A) and (B), the accuracy of the measurements is dependent on the integration time chosen. For a given Δt, the overall uncertainty in dose δD has a signal-to-noise (y-axis) component δD_y and a component δD_x resulting from the uncertainty in time of $\pm\Delta t/2$. We have taken the lowest dose rate MPy/tBuA measurements with $\Delta t = 2$ and 20 s as an example of this. For $\Delta t = 2$ s, we find from the tangential noise $\delta D_y = \pm 0.11$ Gy and $\delta D_x < 0.01$ Gy. For $\Delta t = 20$ s, we find $\delta D_y = \pm 0.01$ Gy and $\delta D_x = \pm 0.04$ Gy. Therefore, the data obtained with the integration time of 20 s provide the more accurate overall measurement with $\delta D = \pm 0.05$ Gy. The optimum value of Δt would in fact have been approximately 10 s for which $\delta D \approx \pm 0.03$ Gy can be estimated.

3.4. Monomer-dependent sensitivity

In figure 9, we compare directly the dose dependences of the fluorescence intensity for MPy solutions in tBuA and MMA for the same dose rate (0.27 Gy min^{-1}) over an accumulated dose range of 2.5 gray, similar to the fractionated doses used in radiotherapy treatment procedures. The much higher sensitivity of the tBuA solution, indicated in the previous sections, is seen to be capable of providing an accurate measure of accumulated dose within this range. The noise level of the tBuA measurements corresponds to an uncertainty in dose of approximately 0.05 gray or about 2% in the maximum dose in figure 10. For the MPy/MMA solution, the uncertainty is approximately a factor of 20 larger, i.e. about 1 gray.

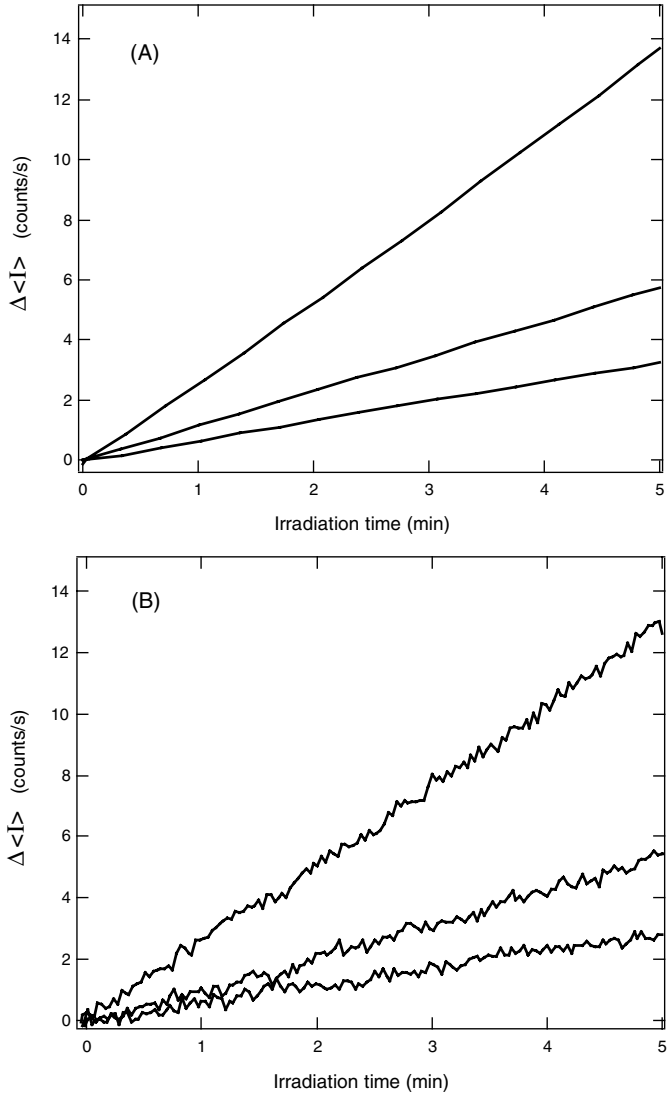

Figure 8. The increase in the fluorescence intensity as a function of time, $\Delta\langle I\rangle$ (see section 3.3), after lowering the probe into the irradiation zone for a solution of MPy in tBuA for dose rates of 3.73, 0.89 and 0.27 Gy min^{-1} (from top to bottom) and total accumulated doses of 19, 4.5 and 1.3 Gy, respectively. In (A), Δt was 20 s and in (B), Δt was 2 s.

Clearly, the MPy/MMA solution is inadequate in the radiotherapy-relevant dose regime. If the concern were with larger total doses, however, as in the case of equipment sterilization or food irradiation, then an MPy/MMA solution would be better suited. This is illustrated by the good linearity displayed by the MPy/MMA solution in figure 10 up to doses of several hundred gray. Even at a total dose of 1 kGy, the deviation is only approximately 5%. At this dose, the monomer conversion is close to 20% and a decrease in the rate of monomer conversion would be expected since the rate of the propagation reaction must decrease. That the decrease is in fact less than 20% is attributed to the increasing viscosity of the medium

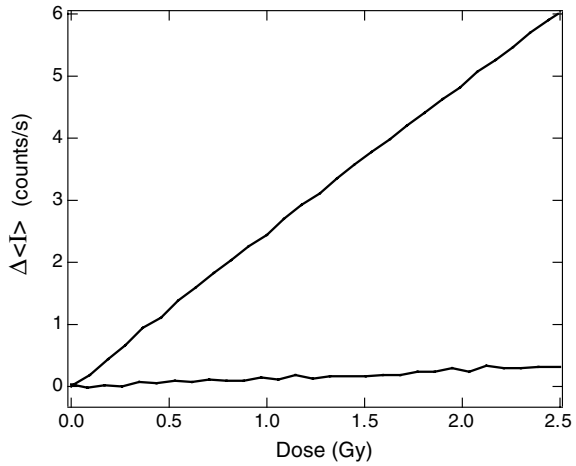

Figure 9. The increase in the fluorescence intensity, $\Delta\langle I\rangle$ (see section 3.3), as a function of dose in the low dose regime for a solution of MPy in MMA, lower plot, and in tBuA, upper plot. The dose rate and integration period were 0.27 Gy min^{-1} and 20 s in both cases.

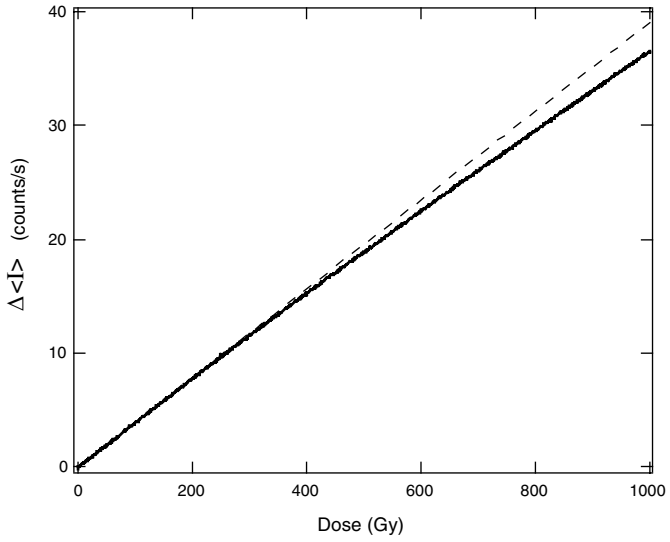

Figure 10. The increase in the fluorescence intensity, $\Delta\langle I\rangle$ (see section 3.3), as a function of dose for a solution of MPy in MMA up to a total dose of 1 kGy. The dose rate was 3.76 Gy min^{-1} and Δt was 20 s. The dashed line represents a linear dependence on dose.

that decreases the rate of radical termination reactions and hence compensates for the slower propagation step.

Solvents with higher sensitivities, using di- or tri-acrylates, or lower sensitivities, using for example the order of magnitude less efficient radiation polymerization of styrene, can be envisaged. In this way, the dynamic range of the measurements could be adjusted to suite the particular application.

3.5. Dose rate dependence

For a pure radiation-polymerizable monomer, the reactions that result in eventual chain termination are second-order, radical–radical combination and disproportionation. The overall reaction mechanism and the derivation of the kinetic solutions for the time and dose dependence of the fractional monomer conversion, ΔC_M, are given in Luthjens *et al* (2000). For low conversion, ΔC_M should increase with irradiation time according to

$$\Delta C_M = P_M (D')^{0.5} t. \tag{1}$$

In (1), D' is the dose rate in Gy s^{-1} and P_M is a parameter that is a characteristic of that particular monomer and is given by

$$P_M = \{k_p [g(R^{\cdot})\rho / 2k_t]^{0.5}\}_M, \tag{2}$$

with k_p and k_t the rate coefficients for propagation and termination, respectively, in units of L $mole^{-1}$ s^{-1}, $g(R^{\cdot})$ the yield of initiating free radicals in moles per joule, and ρ the density in g cm^{-3}.

If the ratio of the efficiency of incorporating a fluorgenic probe molecule into a growing polymer chain to that for incorporating a molecule of the bulk monomer is R_F ($=k_p$[probe]$/k_p$[bulk monomer]), then the fraction of fluorogenic molecules converted to their fluorescent form will be

$$\Delta C_F = R_F P_M (D')^{0.5} t. \tag{3}$$

In the case of MPy in MMA, R_F has been determined to be 1.28 (Frahn *et al* 2001).

Since the intensity of the fluorescence is proportional to the fraction of fluorogenic molecules converted, the slope of a plot of intensity versus time should be linearly dependent on the square root of the dose rate, according to (4), with K_p a constant characteristic of a specific probe, including the particular RFCP solution used:

$$\Delta I(t) = K_p (D')^{0.5} t. \tag{4}$$

In figure 11, the slopes for the time dependences shown in figures 7, 8(A) and (B) are plotted against $\sqrt{D'}$. In all three cases, good linearity is found indicating that spurious chain terminating impurities are absent.

As expected, the data for MPy in tBuA using either a 20 s or 2 s integration period are in good agreement. It is worth mentioning that the two measurement series were carried out using a fresh probe solution for each. This confirms the reproducibility of the preparation procedure. The much lower slope of the plot for MPy in the MMA solution (for which the data points in figure 11 have been multiplied by a factor of 10) reflects the considerably lower value of P_M for MMA compared with tBuA. The tBuA solution is in fact found to be 17 times more sensitive than MMA. This is in agreement with the finding that the propagation rate coefficients for acrylates are in general one to two orders of magnitude larger than those for methacrylates (van Herk 1997). This is attributed to the steric hindrance of the methyl group substituent on the vinyl moiety in methacrylates.

From (4), the dose dependence of the fluorescence is given by

$$\Delta I = K_p D / (D')^{0.5}. \tag{5}$$

The parameter K_p can be determined by measuring the fluorescence in a radiation field of known dose rate D'_S for a given total dose D_S from

$$K_p = \Delta I_S (D'_S)^{0.5} / D_S. \tag{6}$$

Using this 'calibrated' value of K_p, the accumulated dose after an exposure time t in a radiation field of unknown (but constant) dose rate can be determined from

$$D = [\Delta I / K_p]^2 / t. \tag{7}$$

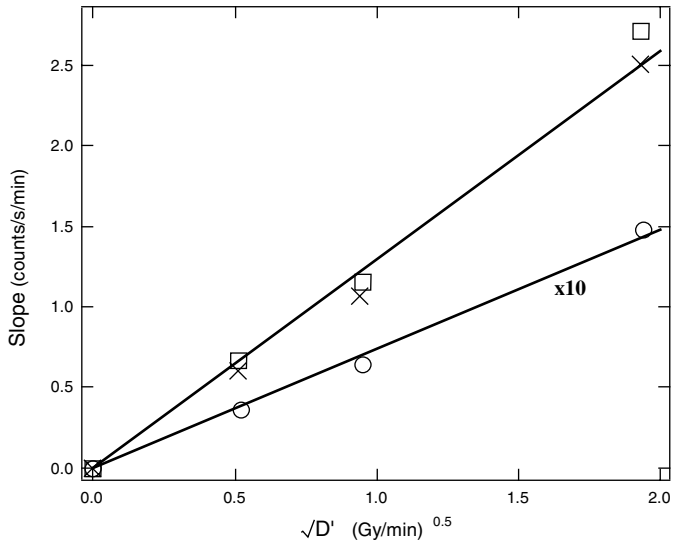

Figure 11. The slopes of the intensity versus time plots shown in figures 7, 8(A) and (B) plotted against the square root of the dose rate: circles, MMA ($\Delta t = 20$ s); squares, tBuA ($\Delta t = 20$ s); crosses, tBuA ($\Delta t = 2$ s). The slopes for MMA have been multiplied by a factor of 10.

In situations where the dose rate is variable in space or time, a dose rate dependence could make interpretation of data using the RFCP complex. That would be the case, for example, for image-guided radiotherapy using multi-leaf-shaped overlapping x-ray beams. We leave a discussion of this potential problem to subsequent reports in which the RFCP effect is applied to multi-dimensional imaging in gel media.

3.6. Dosimetry

The good linear dose dependence and large dynamic range, from tenths of gray up to kilogray depending on the choice of the polymerizable monomer, suggest that RFCP probes may prove to be useful for *in situ* radiation dosimetry using either remote real-time monitoring via optical cables or post-irradiation measurement using sealed, transparent capsules. Advances in the miniaturization of optical devices and wireless transmission technology may even make it possible to apply the RFCP effect to real-time internal dose monitoring during the course of radiotherapeutic treatment. The close to tissue equivalence and the bio-compatibility would be strong plus points in such applications. The lack of the requirement of electrical wiring and applied voltages, necessary for ionization chambers and solid-state diodes, is an advantage common to dosimetry methods based on radiation-induced changes in optical properties.

Of the optical dosimetry methods previously proposed, the aqueous coumarin-3-carboxylic acid solution, mentioned in the introduction, comes closest to the present method (Collins *et al* 1994, Park *et al* 2006). Due to the amplification effect of the polymerization process, which is the basis of our method, the yield of the fluorescent product is however much larger. For example, the *G*-value (molecules per 100 eV) of the fluorescent product in the coumarin-based system is given as 0.12 $(100\ \text{eV})^{-1}$ (Collins *et al* 1994). In the MPy/tBuA solution used in the present study, the yield of the fluorescent polymer product is close to 50 $(100\ \text{eV})^{-1}$ due to the fact that for every free radical produced (*G*-value =

5 $(100\ \text{eV})^{-1}$), 100 000 bulk monomer molecules and 10 MPy molecules are co-polymerized. The added advantage is that the fluorescent product is a high molecular weight polymer, which is important for multi-dimensional dose-imaging applications.

Other optical dosimetric methods are based on radiation-induced changes in absorption (e.g. Fricke solution and radiochromic thin films), prompt radio-luminescence (RIL or 'scintillation'), or thermally or optically stimulated luminescence (TSL or OSL). If we limit the selection to methods capable of real-time *in situ* monitoring, we are left with RIL (Beddar 2007) or OSL (Yukihara and McKeever 2008). Attempting to objectively weigh up the pros and cons of the different methods is almost impossible and to a large extent depends on the efforts that are expended on each technique to bring it to fruition and reduce, if not completely eliminate, the negative aspects.

A distinct disadvantage of the present method is the requirement of an oxygen-free environment for probe preparation. The fact that the fluorescence induced is chemically fixed and cannot be erased could also be seen as a disadvantage, since this would require the use of disposable probes. The dose rate dependence, while fully understood in the present case, is something that will have to be investigated in more detail when practical applications in radiotherapy treatment procedures are considered.

4. Conclusions

In the foregoing, we have demonstrated the efficacy of a novel method of radiation dosimetry based on radio-fluorogenic co-polymerization or RFCP. We have shown that it is possible, using this method, to monitor *in situ*, with a response time of seconds, the accumulated dose in a high-energy radiation field. This can be achieved using a plastic capsule containing less than 0.2 ml of an RFCP solution. Good linear dose dependences are found with a large dynamic range, from a few tenths of a gray up to hundreds of gray, depending on the choice of the radiation-polymerizable monomer used. The method provides a fixed fluorescent record of the total dose delivered which can be read out immediately *in situ* or at a different time and place. The materials used are cheap, can be simply and reproducibly prepared, and are both tissue equivalent and biologically compatible. Even *in vivo* applications may therefore be envisaged.

As mentioned in the introduction, the fluorescent product of RFCP is a high molecular weight polymer. This suggests the possibility of being able to create fixed 2D and 3D fluorescent images of dose distribution using an optically clear, semi-rigid gel matrix containing an RFCP solution. Research into this possible application is ongoing.

References

Beddar A S 2007 Plastic scintillation dosimetry and its application to radiotherapy *Radiat. Meas.* **41** (Suppl. 1) S124–33

Collins A K, Makrigiorgos G M and Svensson G K 1994 Coumarin chemical dosimeter for radiation therapy *Med. Phys.* **21** 1741–7

Collomb-Patton V, Boher P, Leroux T, Fontbonne J-M, Vela A and Batalia A 2009 The DOSIMAP, a high spatial resolution tissue equivalent 2D dosimeter for LINAC QA and IMRT verification *Med. Phys.* **36** 317–28

De Deene Y 2006 On the accuracy and precision of gel dosimetry *J. Phys.: Conf. Ser.* **56** 72–85

d'Errico F 2006 Dosimetric issues in radiation protection of radiotherapy patients *Radiat. Prot. Dosim.* **118** 205–12

Doran S J and Krstajic N 2006 The history and principles of optical computed tomography for scanning 3-D radiation dosimeters *J. Phys.: Conf. Ser.* **56** 45–57

Frahn M S, Luthjens L H and Warman J M 2003 N-(2-anthracene)methacrylamide: a new fluorogenic probe molecule for monitoring *in situ* the radiation-induced polymerization of methyl methacrylate in bulk and solution *Polymer* **44** 7933–8

Frahn M S, Luthjens L H and Warman J M 2004 Time-resolved emission spectra of fluoroprobe and maleimido-fluoroprobe before, during, and after sudden vitrification of radiation-polymerized methyl methacrylate *J. Phys. Chem.* B **108** 2839–45

Frahn M S, Warman J M, Abellon R D and Luthjens L H 2001 Monitoring the radiation-induced bulk polymerization of methyl methacrylate with N-(1-pyrene)maleimide *Radiat. Phys. Chem.* **60** 433–7

Ibbott G S 2006 Clinical applications of gel dosimeters *J. Phys.: Conf. Ser.* **56** 108–31

Jordan K 2006 Review of recent advances in non gel dosimeters *J. Phys.: Conf. Ser.* **56** 132–41

Luthjens L H, Frahn M S, Abellon R D and Warman J M 2000 Steady-state and pulsed studies of the radiation-induced polymerization of methyl methacrylate *Res. Chem. Intermed.* **27** 765–73

Niroomand-Rad A, Blackwell C R, Coursey B M, Gall K P, Galvin J M, McLaughlin W L, Meigooni A S, Nath R, Rodgers J E and Soares C G 1998 Radiochromic dosimetry: recommendations of the AAPM Radiation Therapy Task Group 55 *Med. Phys.* **25** 2093–115

Park M-A, Moore S C, Limpa-Amara N, Kang Z and Makrigiorgos G M 2006 Performance of a coumarin-based liquid dosimeter for phantom evaluations of internal dosimetry *Nucl. Instrum. Methods Phys. Res* A **569** 543–7

Schreiner L J 2006 Dosimetry in modern radiation therapy: limitations and needs *J. Phys.: Conf. Ser.* **56** 1–13

Soares C G 2006 New developments in radiochromic film dosimetry *Radiat. Prot. Dosim.* **120** 100–6

van Herk A M 1997 Pulsed initiation polymerization as a means of obtaining propagation rate coefficients in free-radical polymerizations *J. Macromol. Sci.* C **37** 633–48

Warman J M, Abellon R D, Verhey H J, Verhoeven J W and Hofstraat J W 1997 Maleimido-fluoroprobe: a dual-purpose fluorogenic probe of polymerization dynamics *J. Phys. Chem.* B **101** 4913–6

Warman J M, Abellon R D, Luthjens L H, Suykerbuyk J W A, Verhey H J and Verhoeven J W 1999 *In situ* monitoring of the radiation-induced polymerization of methylmethacrylate using fluorogenic molecular probes *Nucl. Instrum. Methods Phys. Res* B **151** 361–6

Warman J M, Luthjens L H and de Haas M P 2009 *In-situ* radiation dosimetry based on Radio-Fluorogenic Co-Polymerization *J. Phys.: Conf. Ser.* at press

Yukihara E G and McKeever S W S 2008 Optically stimulated luminescence (OSL) dosimetry in medicine *Phys. Med. Biol.* **53** R351–79